Microscopic distribution functions, structure, and kinetic energy of liquid and solid neon: Quantum Monte Carlo simulations

Martin Neumann
Institut für Experimentalphysik der Universität Wien, Strudlhofgasse 4, A-1090 Wien, Austria

Marco Zoppi
Consiglio Nazionale delle Ricerche, Istituto di Elettronica Quantistica, Via Panciatichi 56/30, I-50127 Firenze, Italy
(Received 30 July 2001; published 5 March 2002)

We have performed extensive path integral Monte Carlo simulations of liquid and solid neon, in order to derive the kinetic energy as well as the single-particle and pair distribution functions of neon atoms in the condensed phases. From the single-particle distribution function $n(\mathbf{r})$ one can derive the momentum distribution and thus obtain an independent estimate of the kinetic energy. The simulations have been carried out using mostly the semiempirical HFD-C2 pair potential by Aziz *et al.* [R. A. Aziz, W. J. Meath, and A. R. Allnatt, Chem. Phys. **79**, 295 (1983)], but, in a few cases, we have also used the Lennard-Jones potential. The differences between the potentials, as measured by the properties investigated, are not very large, especially when compared with the actual precision of the experimental data. The simulation results have been compared with all the experimental information that is available from neutron scattering. The overall agreement with the experiments is very good.

DOI: 10.1103/PhysRevE.65.031203 PACS number(s): 61.20.Ja, 61.12.−q, 61.25.Bi, 67.20.+k

I. INTRODUCTION

The properties of the condensed noble gases have been studied thoroughly in the last decades, and many important lessons have been learned from these simple systems. Two well-known concepts that have emerged are the law of corresponding states and the virtual equivalence of the various interatomic pair potentials, on a reduced scale of length and energy. The almost universal use of the Lennard-Jones (LJ) potential is based on this knowledge. In fact, this simple interaction potential not only reproduces the qualitative behavior of condensed matter properties, but it also gives a fair quantitative account of the reality. For example, it is well known that many properties of the heavier noble gases (Ar, Kr, and Xe), including the microscopic structure factor, are reasonably well reproduced by a classical statistical mechanics theory, using simple LJ potentials [1,2]. It is only when pushing the available experimental techniques to the maximum allowed precision that a clear distinction between the LJ potential and a more realistic model can be detected in the microscopic structure function obtained from a neutron diffraction experiment [3,4]. On the other hand, some experimental findings seem to be at variance with these unifying concepts. For example, the lighter noble gases Ne and He cannot be described within the same framework, and this was attributed either to the emergence of quantum mechanical effects or to a poor scaling of the interaction potential.

As a consequence of these facts, the concept of an universal scaling potential was relaxed, and a separate analysis of the interactions of the various noble-gas systems was performed. However, the large amount of work done recently, and the most accurate determinations of the intermolecular interactions in noble-gas systems [5] again lead to the conclusion that the various potentials agree to within 1% on a reduced scale [6]. This leads to the obvious conclusion that, provided the irreducible many-body interactions have negligible effects, the only difference among the various noble-gas systems resides in the magnitude of the quantum effects.

If the scalable potential is assumed to be of the LJ form, then the key parameter that gives a measure of the expected magnitude of quantum effects is the reduced value of the quantum of action h (Planck's constant). This is defined as [7]

$$\Lambda^* = \frac{h}{\sqrt{m\varepsilon\sigma^2}}, \tag{1}$$

where m is the atomic mass, and ε and σ are, respectively, the well depth of the potential and the particle diameter. The quantum parameter Λ^* can also be interpreted as the ratio between the so-called de Boer wavelength [8] and the distance parameter σ of the LJ potential. In a condensed system, where the average intermolecular distance is of the order of σ and the typical interaction energies are of the order of ε, this ratio gives a measure of the relative size of the de Boer wavelength compared to the average interatomic distance. For LJ helium $\Lambda^* = 2.68$, while for neon $\Lambda^* = 0.59$. For argon and the heavier noble-gas systems this value drops significantly, and an essentially classical behavior is expected [9].

As long as N-body statistical mechanics calculations were restricted to classical computer simulations, an effective investigation of the deviation from classical behavior was difficult. Attempts to explain the discrepancies of the microscopic structure of liquid neon have appeared in the literature, and a perturbation method based on the Wigner-Kirkwood (WK) expansion of the quantum mechanical operators was used to resolve the neon anomaly [10,11]. However, the development of genuinely quantum mechanical

methods of computer simulation allows one to tackle the problem more directly. In particular, the powerful path integral Monte Carlo (PIMC) simulation technique has been used to compute the properties of such prototypical quantum systems as normal and superfluid helium [12–14].

At present, the computer simulation machinery is available to evaluate the static equilibrium properties of condensed systems, both on a classical or quantum mechanical level. This may be done by means of classical Metropolis Monte Carlo simulations or by quantum mechanical PIMC. Unfortunately, the development of fully quantum mechanical methods for calculating dynamical properties is still in its infancy. In spite of the numerous attempts made recently to extend the molecular dynamics method to quantum systems [15–21] the general usefulness of the method still has to be demonstrated on an experimental basis.

Apart from the macroscopic thermodynamic and transport properties, the primary experimental access to the collective microscopic features of condensed noble gases is through the radial distribution function $g(r)$ or, to be more precise, its Fourier transform, the structure factor $S(Q)$ [1]. Experiments probing the microscopic dynamic properties are available as well, but their interpretation by means of simulation techniques is limited to the classical ones. However, neutron Compton scattering (NCS), a recently developed experimental technique, provides a direct route to the atomic momentum distribution $n(\mathbf{p})$ whose second moment yields the single-particle kinetic energy E_k [22]. For classical monatomic systems, by the equipartition theorem, $E_k = (3/2)k_B T$, but this value may be substantially exceeded when quantum effects become relevant [23–30]. The momentum distribution of the particles and the expectation value of the kinetic energy are quantities that can be readily computed by PIMC simulation [12]. Thus, even though $n(\mathbf{p})$ is not an intrinsically dynamic property, the possibility of comparing experimental and simulation results for the momentum distribution opens a new direction of research that could have interesting developments in the not too distant future.

The key quantity that may be computed by PIMC is the single-particle density matrix $n(\mathbf{r})$, whose Fourier transform yields the momentum distribution $n(\mathbf{p})$ [31]. For a classical system, $n(\mathbf{p})$ has a Gaussian shape. However, it is known that the simple Gaussian shape is lost for a strongly quantum mechanical system such as ^{4}He in the vicinity of the λ transition [13,32–37], where the emergence of a long-range tail in $n(\mathbf{r})$ is interpreted as a measure of the condensate fraction. One might ask whether significant deviations from a Gaussian distribution are also observable in less strongly quantum mechanical systems. In this context, liquid and solid neon represent an obvious choice.

The properties of liquid and solid neon have been measured, and the available experimental data can be compared with the results of either classical or quantum mechanical simulations. Neutron diffraction experimental data are available, which give the structure factor of liquid neon [38] and thus also the radial distribution function [39]. Moreover, NCS experiments have been published, both for the liquid and the solid phase, which clearly show deviations from the classical value of the kinetic energy [23,24,30]. In the analysis of the experimental data, the shape of the momentum distribution is assumed to be almost Gaussian, and therefore the comparison with the available experimental results was carried out [30] at the level of the width of the distribution, i.e., the translational kinetic energy. However, in a more recent experiment in the liquid phase it is claimed that the momentum distribution is somewhat sharper than the Gaussian [40]. Therefore, one of the aims of the present set of simulations is to investigate the detailed shape of the momentum distribution in a more systematic way.

Previous simulation results exist for the LJ potential, both in the liquid [10,11] and in the solid phase [41,30,42]. These were either classical (in the liquid, using the Wigner-Kirkwood expansion) or quantum simulations (in the solid, using either an effective potential Monte Carlo technique or the PIMC technique). Since the potential model was suspected as a likely cause of the differences found in the comparison with the kinetic energy data of an earlier experiment [23,24,41], we have carried out our simulations using mostly the HFD-C2 potential for neon suggested by Aziz *et al.* [43]. However, a more recent experiment carried out in the solid phase has removed some of the discrepancies and has shown a rather good agreement with the simulations [30,42]. In this paper, we will present a comprehensive comparison of the available experimental data with the present as well as with previous simulation results. This comparison will include virtually all the available data on the kinetic energy and on the pair distribution function.

II. PIMC SIMULATIONS

A. Model potentials and implementation

We have performed an extensive series of simulations of neon (atomic mass 20.183), covering a range of temperatures and densities, both in the liquid and solid phase. Most of the simulations are based on the HFD-C2 [43] pair potential, but a few additional runs were also carried out for the simple Lennard-Jones potential with parameter set $\varepsilon_{LJ} = 36.8$ K and $\sigma_{LJ} = 2.789$ Å [44]. All simulations were performed at constant volume V, temperature T, and number of particles N, and the particles were assumed to obey Boltzmann statistics. Pair interactions were truncated spherically at a distance equal to half the edge length of the cubic simulation box, and potential energies and pressures were corrected in the usual way by integrating over a uniform density beyond the cutoff. Apart from some test runs with smaller systems, we have generally worked with $N = 256$ particles in the liquid and $N = 108$ in the solid. The Trotter number (see below) was varied in the range $P = 4, \ldots, 64$, to monitor the convergence to the quantum mechanical limit.

All our programs are more or less straightforward implementations of the path integral Monte Carlo method [45–47,14] in the canonical ensemble, using the so-called primitive algorithm. As with most variants of PIMC, this is based on a factorization of the N-body density matrix

$$\rho(\mathbf{r}_1^{(1)},\ldots,\mathbf{r}_N^{(1)};\mathbf{r}_1^{(P+1)},\ldots,\mathbf{r}_N^{(P+1)};\beta)=\int\prod_{k=2}^{P}d\mathbf{r}_1^{(k)}\cdots d\mathbf{r}_N^{(k)}\rho(\mathbf{r}_1^{(1)},\ldots,\mathbf{r}_N^{(1)};\mathbf{r}_1^{(2)},\ldots,\mathbf{r}_N^{(2)};\beta/P)$$
$$\times\cdots\rho(\mathbf{r}_1^{(P)},\ldots,\mathbf{r}_N^{(P)};\mathbf{r}_1^{(P+1)},\ldots,\mathbf{r}_N^{(P+1)};\beta/P), \tag{2}$$

which relates the density matrix at temperature $\beta=1/k_BT$ to a convolution of density matrices at the higher temperature β/P. Here, $\mathbf{r}_1,\ldots,\mathbf{r}_N$ are the positions of particles $1,\ldots,N$, and P, the Trotter number, is the number of intermediate states (plus one). In the primitive algorithm, the density matrices at temperature β/P are approximated by their high-temperature limit, in which they factorize into a product of free-particle density matrices and a term containing the intermolecular potential U,

$$\rho(\mathbf{r}_1^{(k)},\ldots,\mathbf{r}_N^{(k)};\mathbf{r}_1^{(k+1)},\ldots,\mathbf{r}_N^{(k+1)};\beta/P)$$
$$\approx\left(\frac{mP}{2\pi\beta\hbar^2}\right)^{3N/2}\prod_{i=1}^{N}\exp\left\{-\frac{mP}{2\beta\hbar^2}[\mathbf{r}_i^{(k+1)}-\mathbf{r}_i^{(k)}]^2\right\}$$
$$\times\exp\left\{\frac{\beta}{2P}[U(\mathbf{r}_1^{(k)},\ldots,\mathbf{r}_N^{(k)})+U(\mathbf{r}_1^{(k+1)},\ldots,\mathbf{r}_N^{(k+1)})]\right\}. \tag{3}$$

Assuming identical, distinguishable particles, the canonical partition function is given by

$$Q=\frac{1}{N!}\int d\mathbf{r}_1\cdots d\mathbf{r}_N\rho(\mathbf{r}_1,\ldots,\mathbf{r}_N;\mathbf{r}_1,\ldots,\mathbf{r}_N;\beta)$$
$$\approx\frac{1}{N!}\left(\frac{mP}{2\pi\beta\hbar^2}\right)^{3NP/2}\int\prod_{k=1}^{P}d\mathbf{r}_1^{(k)}\cdots d\mathbf{r}_N^{(k)}$$
$$\times\exp\left\{-\frac{\beta}{P}\left[\sum_{i=1}^{N}\frac{mP^2}{2\beta^2\hbar^2}\sum_{k=1}^{P}(\mathbf{r}_i^{(k+1)}-\mathbf{r}_i^{(k)})^2+\sum_{k=1}^{P}U(\mathbf{r}_1^{(k)},\ldots,\mathbf{r}_N^{(k)})\right]\right\}. \tag{4}$$

This looks like the configurational partition function, at temperature β/P, of a system of classical ring polymers (labeled $i=1,\ldots,N$), in which successive beads are connected by harmonic springs with spring constant $mP^2/\beta^2\hbar^2$, and where only beads with the same index k are allowed to interact through the intermolecular potential U. For the Trotter (or bead) index k periodic boundary conditions apply, i.e., $\mathbf{r}_i^{(P+1)}=\mathbf{r}_i^{(1)}$.

Expectation values of observables depending only on particle coordinates (but not on their momenta), such as the intermolecular potential energy, the virial, or the pair correlation function $g(r)$, are readily calculated as averages of the general form

$$A(\mathbf{r}_1,\ldots,\mathbf{r}_N)=\frac{1}{Q}\frac{1}{N!}\left(\frac{mP}{2\pi\beta\hbar^2}\right)^{3NP/2}$$
$$\times\int\prod_{k=1}^{P}d\mathbf{r}_1^{(k)}\cdots d\mathbf{r}_N^{(k)}e^{-(\beta/P)\Phi}$$
$$\times\frac{1}{P}\sum_{k=1}^{P}A(\mathbf{r}_1^{(k)},\ldots,\mathbf{r}_N^{(k)}), \tag{5}$$

where Φ is the temperature-dependent potential given by the expression in square brackets in the exponential in Eq. (4). An estimator for the kinetic energy is obtained by applying the thermodynamic relationship $E=\partial(\beta F)/\partial\beta$ to Eq. (4) and subtracting the expectation value of the potential energy. Here, E is the total energy and F is the free energy given by $\beta F=-\ln Q$. The result is

$$E_k=\frac{3NP}{2\beta}-\frac{1}{P}\left\langle\sum_{i=1}^{N}\frac{mP^2}{2\beta^2\hbar^2}\sum_{k=1}^{P}(\mathbf{r}_i^{(k+1)}-\mathbf{r}_i^{(k)})^2\right\rangle. \tag{6}$$

According to this ''crude'' estimator [44] the translational kinetic energy is given by the difference between a constant and the energy stored in the ''intramolecular'' springs.

Both, the primitive algorithm and the crude energy estimator, are sometimes regarded as inefficient and numerically less than optimal [14]. While it is true that using the primitive algorithm rather large Trotter numbers are required to approach the quantum mechanical limit, its principal advantage is the ease of implementation that is comparable to that of a classical monatomic system. Also, in our experience the crude energy estimator is not plagued by excessive fluctuations [48], at least for the Boltzmann systems we have considered so far.

An equally important implementation detail affecting the overall efficiency of the simulation is the strategy for sampling the intramolecular coordinates (i.e., the relative bead positions within a polymer). Since the intramolecular springs usually are extremely stiff compared to the intermolecular potential, random displacements of individual beads are limited to rather smaller step sizes, resulting in a very inefficient sampling of the intramolecular configuration space, even if one uses different displacements for individual beads and the center of mass of the polymer. Therefore, in all our simulations involving closed ring polymers (but not in the simulations involving open polymers described in Sec. II C), we have sampled the intramolecular coordinates directly from the free-particle density matrix [the contribution to the Boltzmann factor originating from the first term in the exponential in Eq. (4)], so that each single-particle move consists of an independently sampled *complete* set of intramolecular co-

TABLE I. PIMC simulations of liquid neon with the HFD-C2 pair potential and $N=256$ particles. P is the number of beads on the classical ring polymers (Trotter number), x_A the fraction of accepted trial moves (acceptance ratio), and R the rms radius of the ring polymers. E_k and U are the kinetic and potential energies, and p is the pressure. Values in parentheses are from simulations with the Lennard-Jones potential. The statistical errors on the kinetic energy are of the order of a few units in 10^{-2} K and appear to slightly increase with the Trotter number. Typical errors on the quantum mechanical limits are estimated to be below 0.1 K, i.e., much smaller than the available experimental errors.

ρ (nm^{-3})	T (K)	P	Passes	x_A	R (Å)	E_k/N (K)	U (kJ/mol)	p (atm)
31.70	35.3	4	250 000	0.335	0.124	59.31	−1.460	−43
		8	250 000	0.335	0.127	60.03	−1.457	−38
		16	250 000	0.335	0.128	60.37	−1.456	−37
		32	250 000	0.335	0.129	60.34	−1.456	−36
		(32)	(500 000)	(0.339)	(0.129)	(60.25)	(−1.450)	(20)
		Expt.				66.4±3.3		21
34.61	35.1	4	250 000	0.480	0.123	60.20	−1.595	42
		8	250 000	0.482	0.127	61.09	−1.591	48
		16	250 000	0.482	0.128	61.38	−1.590	52
		32	250 000	0.482	0.129	61.44	−1.592	51
		(32)	(500 000)	(0.482)	(0.129)	(61.39)	(−1.576)	(145)
		Expt.				69.0±4.7		137
36.28	25.8	4	250 000	0.466	0.141	47.85	−1.735	−144
		8	250 000	0.470	0.147	49.19	−1.730	−131
		16	250 000	0.472	0.148	49.60	−1.728	−128
		32	250 000	0.472	0.148	49.72	−1.729	−127
		(32)	(500 000)	(0.471)	(0.148)	(49.76)	(−1.707)	(−9)
		Expt.				52.8±3.7		1

ordinates and a random displacement of the polymer's center of mass. To be consistent with this sampling scheme, the Metropolis criterion for the acceptance or rejection of the trial move now only involves the difference in *intermolecular* energies, since the intramolecular part has been factored out from the probability density. The free-particle density matrix itself is most conveniently sampled by transforming the intramolecular coordinates in such a way that the resulting probability density is a product of $P-1$ independent Gaussians. This has the additional advantage of isolating the center of mass of the polymer as an independent uniform random variable for which rather large displacements can be made. The required transformation is not unique, but one obvious choice is the Fourier transform used to diagonalize the linear chain in elementary solid state physics. We have found that PIMC based on the direct sampling of the free-particle density matrix is a very efficient implementation as long as the spread of the free particle is not appreciably larger than the extent of the single-particle density matrix in the condensed phase. In that case the rate of accepted moves drops to a low value (cf. the lowest temperature simulation of the solid in Table II).

B. Thermodynamic states

The thermodynamic conditions and the details of our PIMC simulations in the liquid phase are summarized in Table I. The density and temperature of each state point were chosen to match the experimental conditions of Ref. [23]. Each simulation was started either from a random configuration or a perfect fcc lattice of $N=256$ quantum particles (represented by classical ring polymers with Trotter numbers in the range $P=4,\ldots,32$) and consisted of an equilibration stage of $20\,000\times M$ passes (attempted moves per particle), followed by a production stage of at least $50\,000\times M$ passes. Here M is the "dilution factor," i.e., the number of passes performed before analyzing the next configuration. In the present simulations we have always used $M=5$. In Table I, x_A is the acceptance ratio, i.e., the fraction of accepted trial moves, R is the rms spread of the ring polymers, E_k is the kinetic energy, U is the potential energy, and p is the pressure.

It is interesting to note that the size of the quantum effects in the liquid phase, even though not negligible, is not very large, as is evident from the comparison between the kinetic energy per particle and the classical limit $(3/2)k_BT$. Another indication of the moderate role of quantum mechanics at these relatively high temperatures is the fast convergence of the various thermodynamic quantities with the Trotter number P. This is a consequence of the fact that R, the positional "spread" of the quantum particles, is at most 5% of the atomic diameter. While all other entries in the table are for the HFD-C2 potential, the results shown in parentheses (for

$P=32$ only) were obtained using the LJ model. We observe that the only significant difference between the two potentials is in the results for the pressure, with the LJ values being consistently much closer to the experimental ones. Since the HFD-C2 pair potential, by construction, is superior to LJ in describing the experimental pair properties, this fact may be interpreted as an indication that the LJ model effectively accounts for irreducible three-body and higher-order interactions.

The thermodynamic conditions and the details of our simulations in the solid phase are collected in Table II. Since there are no experimental pair correlations available for comparison and there was thus no need to calculate the long-range structure, we limited the number of particles in the solid to $N=108$, but extended the variation of the Trotter number to the range $P=4,\ldots,64$. The density and temperature of each state point were now chosen to match the experimental conditions of Refs. [24] and [30]. As before, each simulation was started from a perfect fcc lattice and equilibrated for $20\,000\times M$ passes, with the dilution factor again set to $M=5$. In order to compensate for the loss in statistical information (due to the lower number of particles compared to the previous set of simulations), the production stage was extended to at least $100\,000\times M$ passes. At the lowest temperature, where the acceptance rate for direct sampling from the free-particle density matrix drops by an order of magnitude, the runs with the highest Trotter numbers were substantially longer.

Some of the simulations in the solid phase are characterized by a much lower temperature than in the liquid. Therefore, one may expect considerably larger quantum effects, and this is the reason why we have extended the maximum Trotter number from $P=32$ to 64. The results in Table II confirm this expectation. For instance, we find that when the temperature is lowered from $T=26.4$ to 4.7 K, the kinetic energy per particle decreases only from 54 to 41 K, thus deviating more and more from the classical equipartition theorem and approaching the ground state value. As in the case of the liquid, the entries given in parentheses were obtained from additional runs with the LJ potential and are generally close to the results for the HFD-C2 model. Substantial differences are only found for the pressure, where the LJ potential again outperforms HFD-C2, although the absolute values obtained with such small systems are probably not too reliable.

C. The single-particle density matrix

The single-particle density matrix for our system of identical particles obeying Boltzmann statistics may be defined as

$$n(\mathbf{r})=\frac{1}{Q}\frac{1}{N!}\int d\mathbf{r}_1\cdots d\mathbf{r}_N \times\rho(\mathbf{r}_1,\mathbf{r}_2,\ldots,\mathbf{r}_N;\mathbf{r}_1+\mathbf{r},\mathbf{r}_2,\ldots,\mathbf{r}_N;\beta). \quad (7)$$

Its Fourier transform is the single-particle momentum distribution,

$$n(\mathbf{p})=\frac{1}{(2\pi\hbar)^3}\int d\mathbf{r}e^{-(i/\hbar)\mathbf{p}\cdot\mathbf{r}}n(\mathbf{r}), \quad (8)$$

which is a properly normalized distribution function, while the normalization of $n(\mathbf{r})$ is such that $n(0)=1$. In the classical limit both functions reduce to Gaussians: the familiar Maxwell distribution of momenta

$$n(\mathbf{p})=\left(\frac{\beta}{2\pi m}\right)^{3/2}e^{-\beta(p^2/2m)}, \quad (9)$$

and

$$n(\mathbf{r})=e^{-(mr^2/2\beta\hbar^2)}. \quad (10)$$

In the analysis of neutron Compton scattering experiments it is usually assumed that $n(\mathbf{p})$ is Gaussian also for quantum mechanical systems, so that the single-particle kinetic energy may be obtained from the width of a Gaussian fitted to $n(\mathbf{r})$ or $n(\mathbf{p})$, e.g.,

$$n(\mathbf{r})=\exp\left(-\frac{m(E_k/N)}{3\hbar^2}r^2\right). \quad (11)$$

Path integral Monte Carlo simulations, at least in their conventional implementation, only allow the calculation of averages for which knowledge of the diagonal elements of the density matrix is sufficient. This covers the majority of cases in which only thermodynamic or structural information is sought. On the other hand, the calculation of $n(\mathbf{r})$ also requires information about the off-diagonal elements. Therefore, in their first calculation by PIMC of the single-particle density matrix of normal and superfluid helium, Ceperley and Pollock [13] proposed two complementary methods to determine $n(\mathbf{r})$ by simulation.

In the first approach ("virtual displacements"), advantage is taken of the fact that Eq. (7), after performing a factorization to temperature β/P and replacing the last factor by $\rho(\mathbf{r}_1^{(P)},\ldots;\mathbf{r}_1^{(1)},\ldots;\beta/P)\times[\rho(\mathbf{r}_1^{(P)},\ldots;\mathbf{r}_1^{(1)}+\mathbf{r},\ldots;\beta/P)/\rho(\mathbf{r}_1^{(P)},\ldots;\mathbf{r}_1^{(1)},\ldots;\beta/P)]$, may be written as

$$n(\mathbf{r})=\left\langle\frac{\rho(\mathbf{r}_1^{(P)},\ldots;\mathbf{r}_1^{(1)}+\mathbf{r},\ldots;\beta/P)}{\rho(\mathbf{r}_1^{(P)},\ldots;\mathbf{r}_1^{(1)},\ldots;\beta/P)}\right\rangle \quad (12)$$

or, in the primitive algorithm,

$$n(\mathbf{r})\approx\left\langle\exp\left(-\frac{\beta}{P}\left\{\frac{mP^2}{2\beta^2\hbar^2}[(\mathbf{r}_1^{(1)}+\mathbf{r}-\mathbf{r}_1^{(P)})^2-(\mathbf{r}_1^{(1)}-\mathbf{r}_1^{(P)})^2]+\frac{1}{2}[U(\mathbf{r}_1^{(1)}+\mathbf{r},\mathbf{r}_2^{(1)},\ldots,\mathbf{r}_N^{(1)})-U(\mathbf{r}_1^{(1)},\mathbf{r}_2^{(1)},\ldots,\mathbf{r}_N^{(1)})]\right\}\right)\right\rangle. \quad (13)$$

This is interpreted as an average, over all configurations of *closed* ring polymers, in which bead 1 of polymer 1 is vir-

TABLE II. PIMC simulations of solid neon with the HFD-C2 pair potential and $N=108$ particles. P is the number of beads on the classical ring polymers (Trotter number), x_A the fraction of accepted trial moves (acceptance ratio), and R the rms radius of the ring polymers. E_k and U are the kinetic and potential energies, and p is the pressure. Values in parentheses are from simulations with the Lennard-Jones potential. The statistical errors on the kinetic energy are of the order of a few units in 10^{-2} K and appear to slightly increase with the Trotter number. Typical errors on the quantum mechanical limits are estimated to be below 0.1 K, i.e., much smaller than the available experimental errors.

ρ (nm^{-3})	T (K)	P	Passes	x_A	R (Å)	E_k/N (K)	U (kJ/mol)	p (atm)
43.26	26.4	4	500 000	0.473	0.138	51.68	−2.180	−107
		8	500 000	0.478	0.144	53.36	−2.172	−77
		16	500 000	0.481	0.145	53.91	−2.171	−69
		32	500 000	0.481	0.145	54.07	−2.170	−67
		(32)	(500 000)	(0.474)	(0.145)	(54.45)	(−2.103)	(211)
		64	500 000	0.681	0.146	54.00	−2.170	−67
		Expt.				57.9±2.0		170
43.91	20.2	4	500 000	0.480	0.153	44.23	−2.260	−255
		8	500 000	0.492	0.160	46.79	−2.248	−204
		16	500 000	0.497	0.162	47.61	−2.244	−190
		32	500 000	0.498	0.163	47.84	−2.243	−186
		(32)	(500 000)	(0.490)	(0.163)	(48.21)	(−2.168)	(113)
		64	500 000	0.499	0.163	47.94	−2.243	−185
		Expt.				48±1		
44.12	17.8	4	500 000	0.433	0.160	41.45	−2.288	−313
		8	500 000	0.445	0.168	44.47	−2.273	−249
		16	500 000	0.451	0.170	45.48	−2.268	−229
		32	500 000	0.453	0.171	45.85	−2.267	−223
		(32)	(500 000)	(0.445)	(0.171)	(46.17)	(−2.189)	(80)
		64	500 000	0.454	0.172	45.81	−2.267	−222
		Expt.				51.2±2.8		0.01
44.68	10.2	4	500 000	0.310	0.184	32.24	−2.370	−503
		8	500 000	0.324	0.200	38.08	−2.338	−355
		16	500 000	0.324	0.205	40.65	−2.325	−297
		32	500 000	0.331	0.207	41.48	−2.321	−278
		(32)	(500 000)	(0.320)	(0.206)	(41.90)	(−2.236)	(39)
		64	500 000	0.332	0.207	41.70	−2.319	−273
		Expt.				43±1		
44.77	11.4	4	500 000	0.301	0.180	34.04	−2.365	−440
		8	500 000	0.372	0.194	39.35	−2.334	−308
		16	500 000	0.388	0.198	41.58	−2.322	−258
		32	500 000	0.394	0.200	42.28	−2.320	−243
		(32)	(500 000)	(0.383)	(0.199)	(42.67)	(−2.234)	(75)
		64	500 000	0.396	0.200	42.43	−2.319	−239
		Expt.				49.0±2.4		1
44.87	9.4	4	500 000	0.248	0.186	31.23	−2.385	−507
		8	500 000	0.256	0.203	37.63	−2.349	−341
		16	500 000	0.270	0.209	40.59	−2.333	−270
		32	500 000	0.276	0.211	41.59	−2.328	−249
		(32)	(500 000)	(0.266)	(0.210)	(41.99)	(−2.241)	(73)

TABLE II. (*Continued*).

ρ (nm^{-3})	T (K)	P	Passes	x_A	R (Å)	E_k/N (K)	U (kJ/mol)	p (atm)
		64	500 000	0.278	0.211	41.84	−2.327	−242
		Expt.				49.1±4.0		1
44.97	4.7	4	500 000	0.028	0.191	21.40	−2.453	−792
		8	500 000	0.018	0.224	30.52	−2.395	−515
		16	500 000	0.018	0.237	36.96	−2.357	−342
		32	4 000 000	0.019	0.241	40.02	−2.341	−271
		(32)	(2 500 000)	(0.017)	(0.241)	(40.42)	(−2.253)	(51)
		64	2 500 000	0.020	0.242	41.07	−2.336	−247
		Expt.				49.2±2.8		1

tually displaced to a distance $\mathbf{r}$ away from its original position $\mathbf{r}_1^{(1)}$. Equivalently, one may say that the polymer is virtually cut between beads P and 1, a $(P+1)$th bead is created at position $\mathbf{r}_1^{(1)}+\mathbf{r}$ and connected to bead P (but not 1), and the ratio of the density matrices for the open/closed polymer is averaged. Since not only bead 1 on polymer 1, but any of the $N\times P$ equivalent particles may be displaced, this method would appear to be simple and extremely efficient. In practice, however, it is only of very limited use, because in any simulation (of finite duration) with closed polymers, beads 1 and P will always be very close together—the more so the higher the Trotter number P (in the primitive algorithm the spring constants are proportional to $1/P$). Consequently, virtual bead $P+1$, which is linked to P by a similar stiff spring, cannot be far from bead 1 either, and $n(\mathbf{r})$ will be affected by large errors as soon as $\mathbf{r}$ gets appreciably larger than the typical distance between successive beads on a ring polymer.

Therefore, in the second approach (''open polymer'') proposed by Ceperley and Pollock [13], one rewrites Eq. (7) as

$$n(\mathbf{r})=\frac{1}{Q}\frac{1}{N!}\int d\mathbf{r}_1\cdots d\mathbf{r}_N d\mathbf{r}_1'\,\delta^{(3)}[\mathbf{r}_1'-(\mathbf{r}_1+\mathbf{r})] \times\rho(\mathbf{r}_1,\mathbf{r}_2,\ldots;\mathbf{r}_1',\mathbf{r}_2,\ldots;\beta), \tag{14}$$

introducing an additional integration variable $\mathbf{r}_1'$. Factorization of the density matrix yields

$$n(\mathbf{r})=\frac{1}{Q}\frac{1}{N!}\int\prod_{k=1}^{P}\{d\mathbf{r}_1^{(k)}\cdots d\mathbf{r}_N^{(k)}\}d\mathbf{r}_1^{(P+1)}\delta^{(3)}[\mathbf{r}_1^{(P+1)} -(\mathbf{r}_1^{(1)}+\mathbf{r})]\rho(\mathbf{r}_1^{(1)},\mathbf{r}_2^{(1)},\ldots;\mathbf{r}_1^{(2)},\mathbf{r}_2^{(2)},\ldots;\beta/P) \times\cdots\times\rho(\mathbf{r}_1^{(P)},\mathbf{r}_2^{(P)},\ldots;\mathbf{r}_1^{(P+1)},\mathbf{r}_2^{(1)},\ldots;\beta/P), \tag{15}$$

and, specifically in the case of the primitive algorithm,

$$n(\mathbf{r})\approx\frac{1}{Q}\frac{1}{N!}\left(\frac{mP}{2\pi\hbar^2}\right)^{(3NP/2)}\int\prod_{k=1}^{P}\{d\mathbf{r}_1^{(k)}\cdots d\mathbf{r}_N^{(k)}\} \times d\mathbf{r}_1^{(P+1)}\delta^{(3)}[\mathbf{r}_1^{(P+1)}-(\mathbf{r}_1^{(1)}+\mathbf{r})] \times\exp\left\{-\frac{\beta}{P}\left[\frac{mP^2}{2\beta^2\hbar^2}\sum_{k=1}^{P}(\mathbf{r}_1^{(k+1)}-\mathbf{r}_1^{(k)})^2 +\sum_{i=2}^{N}\frac{mP^2}{2\beta^2\hbar^2}\sum_{k=1}^{P}(\mathbf{r}_i^{(k+1)}-\mathbf{r}_i^{(k)})^2\right]\right\} \times\exp\left\{-\frac{\beta}{P}\left[\frac{1}{2}U(\mathbf{r}_1^{(P+1)},\ldots,\mathbf{r}_N^{(1)}) +\frac{1}{2}U(\mathbf{r}_1^{(1)},\ldots,\mathbf{r}_N^{(1)})+\sum_{k=2}^{P}U(\mathbf{r}_1^{(k)},\ldots,\mathbf{r}_N^{(k)})\right]\right\}. \tag{16}$$

Here, the arguments of the exponentials have been written as the sum of two (or three) terms to indicate that bead coordinates are periodic with respect to k only in the last term but not in the first (and second) term(s). In other words, for polymer 1, $\mathbf{r}_1^{(P+1)}$ is an independent variable with $\mathbf{r}_1^{(P+1)}\neq\mathbf{r}_1^{(1)}$. Thus, apart from a normalization factor (Q is still the partition function of the original ring polymer system), $n(\mathbf{r})$ may be obtained from the end-to-end distribution of a *single open polymer* consisting of $P+1$ beads, embedded in a system of $N-1$ closed ring polymers. Because of the unknown normalization factor the resulting distribution is not automatically normalized to $n(0)=1$, but this is generally not a problem, as one is usually only interested in the shape of $n(\mathbf{r})$. A more serious drawback is the fact that the open polymer method requires much longer simulations than virtual displacements, because only a single polymer (with a single end-to-end distance) is available for averaging. Also, because $\mathbf{r}=\mathbf{r}_1^{(1)}-\mathbf{r}_1^{(P+1)}$ is a three-dimensional vector, intermediate end-to-end distances are sampled much more frequently than small ones, leading to rather poor statistics at very low $\mathbf{r}$. This may be overcome by introducing a weighting function

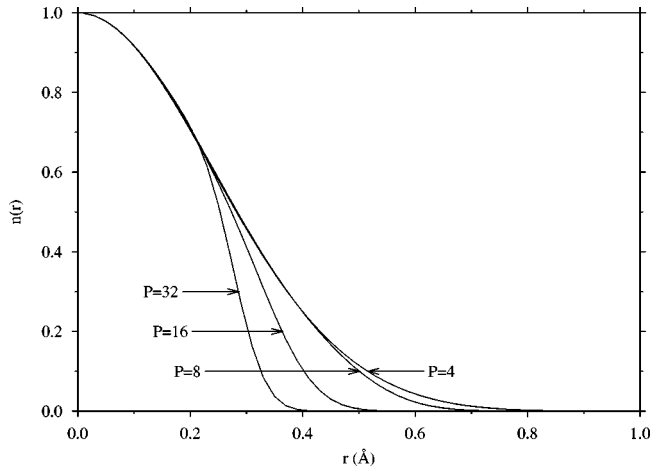

FIG. 1. Single-particle density matrix obtained with the virtual displacement algorithm for liquid neon at $\rho=34.61$ nm^{-3}, $T=35.1$ K. The number of (Lennard-Jones) particles was $N=108$, and P is the number of beads on the classical ring polymers.

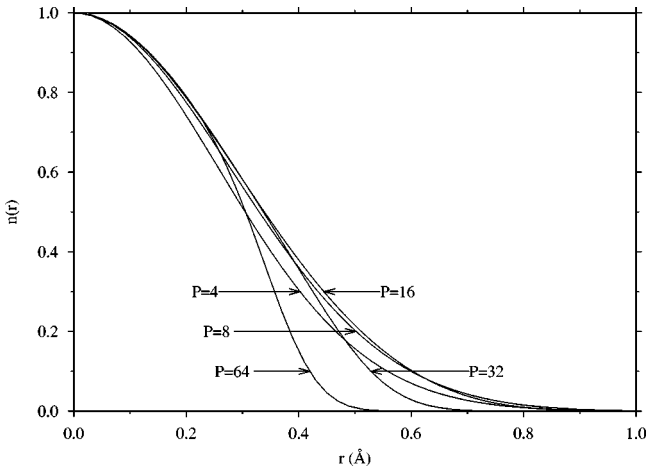

FIG. 2. Single-particle density matrix obtained with the virtual displacement algorithm for solid neon at $\rho=44.87$ nm^{-3}, $T=9.4$ K. The number of (Lennard-Jones) particles was $N=108$, and P is the number of beads on the classical ring polymers.

that increases the sampling rate at low $\mathbf{r}$, but we have not found this necessary in the present paper.

D. Test of the Gaussian assumption

The relative merits of the two methods for calculating $n(\mathbf{r})$ and the principal features of the single-particle density matrix have already been discussed by Ceperley and Pollock [13]. In particular, these authors found that the methods were complementary, with virtual displacements being very efficient for small $\mathbf{r}$ and the open polymer algorithm superior at long range, so that the respective curves could be matched in the intermediate range. As to the shape of $n(\mathbf{r})$, small but significant deviations from the Gaussian form were observed. However, these conclusions were based on simulations of normal and superfluid helium near the λ transition and do not necessarily carry over to a considerably less quantum mechanical system such as neon.

Therefore, and because the assumption of a Gaussian momentum distribution is at the heart of the experimental approach to the kinetic energy, we decided to perform a systematic investigation of $n(\mathbf{r})$ for neon at two selected thermodynamic states. At the same time, this would also allow us to study the convergence, within either algorithm, of $n(\mathbf{r})$ with the Trotter number P. In all these simulations, neon was modeled as a Lennard-Jones system, and the thermodynamic states considered were one typical of the liquid ($\rho=34.61$ nm^{-3}, $T=35.1$ K) and one in the solid phase ($\rho=44.87$ nm^{-3}, $T=9.4$ K). Runs employing virtual displacements were typically 0.5×10^6 passes long, simulations based on the open polymer algorithm consisted of 10^7 passes. In the latter case, intramolecular configurations were not sampled directly (from the free-particle density maxtrix), but by the ''slow'' method, i.e., combining small simultaneous random displacements of a polymer's beads with a larger displacement of its center of mass and subjecting this trial configuration to the usual Metropolis acceptance criterion. Since neither the kinetic energy nor $n(\mathbf{r})$ should be strongly N dependent, some calculations were performed with rather small system sizes.

Figure 1 shows the single-particle density matrix in the liquid, as obtained with a system of $N=108$ particles and Trotter numbers in the range $P=4,\ldots,32$. (Note that, in an isotropic system, $n(\mathbf{r})$ can only depend on the magnitude of $r=|\mathbf{r}|$.) As can be seen, the width of $n(\mathbf{r})$ is only 0.25–0.3 Å (about a factor of 5 smaller than in liquid helium), but the results are clearly not convergent with P: while the curves for $P=4$ and 8 are still rather similar (and approximately Gaussian in shape), the $P=16$ and 32 results are dramatically different, and the effective range of $n(\mathbf{r})$ seems to shrink systematically with P. Thus, apart from an initial portion, where all curves nicely superimpose, the shape of $n(\mathbf{r})$ is completely undefined.

In the solid, Fig. 2 (again based on simulations with $N=108$ particles), the situation is similar, except that at this lower temperature the apparent width of $n(\mathbf{r})$ initially seems to increase and approach a stable value around $P=8$ or 16, before eventually following the same pattern as in the liquid. As already indicated in Sec. II C, this failure of the virtual displacement method is caused by the fact that, on a closed ring polymer, large displacements of a virtual particle (far) away from bead 1 have an increasingly low probability when both the virtual particle and bead 1 are linked by their respective springs to a common bead P. This systematic underestimate of $n(\mathbf{r})$ at long range is particularly severe for an unsophisticated PIMC implementation such as the primitive algorithm, where one is forced to go to rather large Trotter numbers, but in principle this problem might also be present in other implementations. Therefore, we have to conclude that the virtual displacement method is not suitable for establishing the shape of $n(\mathbf{r})$, except in a very limited range around $\mathbf{r}=0$. On the other hand, for $\mathbf{r}\to0$, the behavior of $n(\mathbf{r})$ is more readily obtained from a direct estimate of the kinetic energy,

$$n(\mathbf{r})=n(0)+\frac{r^2}{2}\nabla^2 n(\mathbf{r})\big|_{\mathbf{r}=0}+\cdots=1-\frac{m(E_k/N)}{3\hbar^2}r^2+\cdots, \tag{17}$$

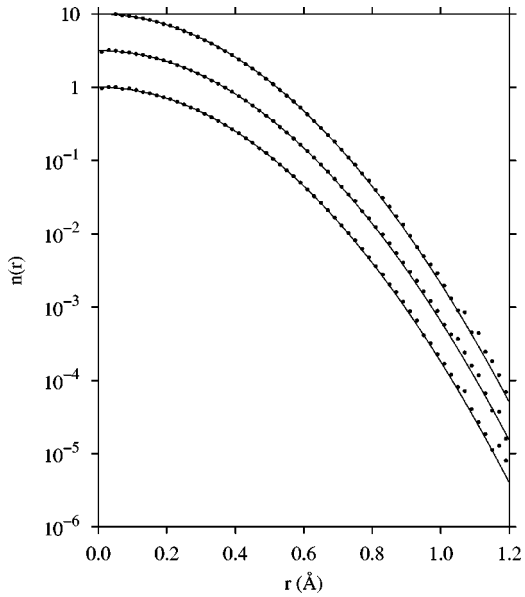

FIG. 3. Single-particle density matrix obtained with the open polymer algorithm for liquid neon at $\rho=34.61$ nm^{-3}, $T=35.1$ K. Circles, distribution of end-to-end distances for an open polymer with $P+1$ beads embedded in a system of $N-1$ closed ring polymers; solid lines, r^2-weighted fit of a Gaussian to the raw data. The total number of (Lennard-Jones) particles was $N=108$, and P is the number of beads on the closed ring polymers. The plots have been shifted for clarity ($P=4$, 8, and 16, from bottom to top).

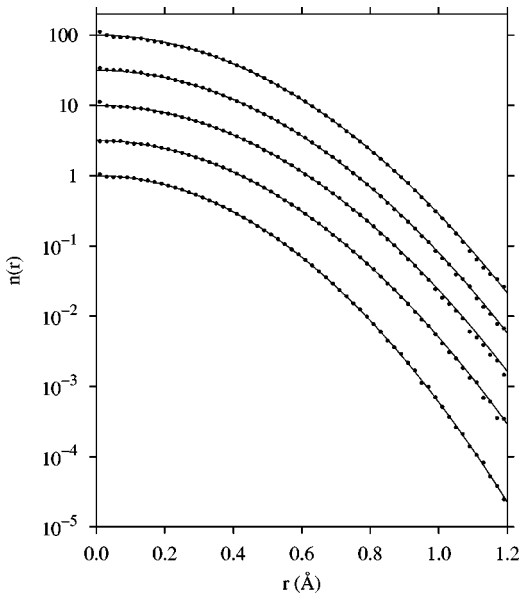

FIG. 4. Single-particle density matrix obtained with the open polymer algorithm for solid neon at $\rho=44.87$ nm^{-3}, $T=9.4$ K. Circles, distribution of end-to-end distances for an open polymer with $P+1$ beads embedded in a system of $N-1$ closed ring polymers; solid lines, r^2-weighted fit of a Gaussian to the raw data. The total number of (Lennard-Jones) particles was $N=32$, and P is the number of beads on the closed ring polymers. The plots have been shifted for clarity ($P=4$, 8, 16, 32, and 64, from bottom to top).

a relationship that is independent of the Gaussian assumption.

Of the two problems associated with the open polymer algorithm, namely, (i) that the calculated probability density of end-to-end distances does not yield a properly normalized $n(\mathbf{r})$, and (ii) that small end-to-end distances are not sampled effectively, the former seems easier to fix than the latter. However, as Fig. 6 (see below) shows, it is precisely because of the large scatter of the data points at small $\mathbf{r}$, that we cannot normalize the simulation results by simply dividing through by the $\mathbf{r}=0$ value. On the other hand, if the functional form of $n(\mathbf{r})$ were known, both problems could be solved simultaneously by fitting a function of this type to the raw data. This would not only smooth the scatter of the data points but also provide a clean value at $\mathbf{r}=0$.

Since, for neon, $n(\mathbf{r})$ seems to be Gaussian to a very good approximation, we have followed this procedure in the present paper, i.e., a *normalized* Gaussian,

$$n'(\mathbf{r})=\left(\frac{m(E_k/N)}{3\pi\hbar^2}\right)^{3/2}\exp\left(-\frac{mE_k/N}{3\hbar^2}r^2\right), \qquad (18)$$

was fitted to the raw data, which was then divided by the prefactor of the exponential to yield a properly normalized $n(\mathbf{r})$. Actually, it was not $n'(\mathbf{r})$ but $r^2n'(\mathbf{r})$ that was fitted to the data, in order to suppress the influence of the points with the largest uncertainty near $\mathbf{r}=0$; this is also consistent with the relative frequency of counts in the end-to-end distance histograms. The fitting parameter E_k may be regarded as an independent estimate of the kinetic energy.

The results obtained in this way are shown in Fig. 3 (liquid; $N=256$ particles with Trotter numbers $P=4$, 8, and 16) and Fig. 4 (solid; $N=32$ particles and Trotter numbers in the range $P=4,\ldots,64$). As can be seen, for neon the assumption that $n(\mathbf{r})$ is Gaussian holds over four or five orders of magnitude, and this seems to be true for both the liquid and the solid phases, at least under the thermodynamic conditions we have studied. What is even more striking—and in contrast to the results of the virtual displacement method—is the fact that, with the open polymer algorithm, $n(\mathbf{r})$ is Gaussian not only in the quantum mechanical limit, but also for all finite values of P. In the liquid, the $P=4$, 8, and 16 curves are so similar that they would be indistinguishable on the scale of the plot if they were superimposed. In the solid, the widths of the curves do change slightly with P, but their shape is Gaussian for all P.

The convergence of $n(\mathbf{r})$ to a limiting form is also examined, on a linear scale, in Fig. 5. (For clarity, only the fitted curves but not the raw data are shown.) In contrast to Fig. 2, the curves for the various P now show a consistent pattern: the width of $n(\mathbf{r})$ increases monotonically with P, and a well-defined limit seems to be approached as $P\rightarrow\infty$.

A final comparison of the algorithms for calculating $n(\mathbf{r})$, including raw and fitted data for the highest Trotter numbers in the liquid and solid phases, is made in Fig. 6. This figure not only illustrates the difficulty of obtaining reliable small $\mathbf{r}$ data with the open polymer algorithm, but also justifies our

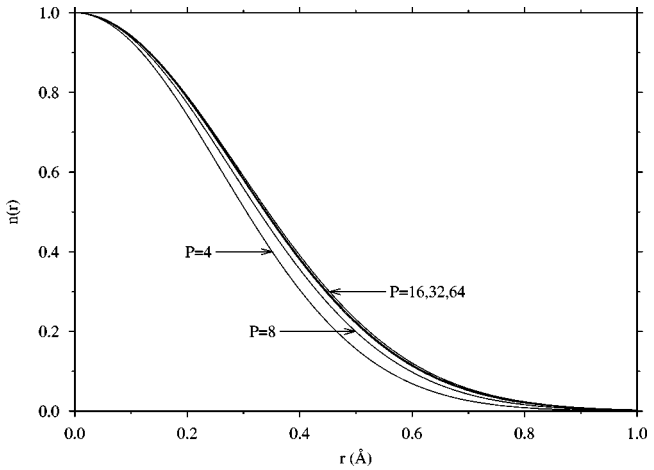

FIG. 5. Single-particle density matrix obtained with the open polymer algorithm for solid neon at $\rho=44.87$ nm^{-3}, $T=9.4$ K. Only the Gaussians fitted to the raw data are shown. The total (open plus closed polymers) number of LJ particles was $N=32$, and P is the number of beads on the closed ring polymers.

procedure of fitting Gaussians to the raw data. Since the points at small $\mathbf{r}$ were given relatively little weight, there are considerable deviations between data and fits in this range. Nevertheless, the fitted Gaussians are in excellent agreement with the curves obtained with the virtual displacement method for $r<0.15$ Å, i.e., in the range where the latter method is expected to perform best. On the other hand, the $n(\mathbf{r})$'s from the virtual displacement method are again found to fail badly for $r>0.25$ Å. Since, in this example, the solid is at a much lower temperature (9.4 K) than the liquid (35.1 K), its kinetic energy is also lower, and its momentum distribution narrower. Consequently, $n(\mathbf{r})$, the Fourier transform

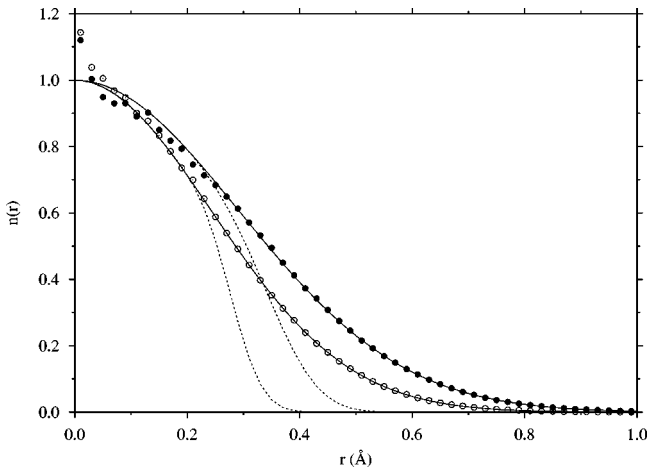

FIG. 6. Single-particle density matrix obtained by various methods for liquid and solid neon. Open circles, normalized end-to-end distribution of an open polymer in the liquid ($\rho=34.61$ nm^{-3}, $T=35.1$ K, $N=256$ $P=16$); full circles, normalized end-to-end distribution in the solid ($\rho=44.87$ nm^{-3}, $T=9.4$ K, $N=32$, $P=64$); solid lines, Gaussians fitted to the raw data; dashed lines, results of the virtual displacement algorithm for the liquid ($N=108$, $P=32$) and the solid ($N=108$, $P=64$).

TABLE III. Comparison of different methods of calculating the kinetic energy of LJ neon, for typical states in the liquid and solid phase. Fifth column, fit of a normalized Gaussian to the r^2-weighted single-particle density matrix; sixth column, E_k as obtained from the crude energy estimator (intramolecular spring energy). N is the number of Lennard-Jones particles, P the Trotter number, and the results are based on simulations of 10^7 passes.

ρ (nm^{-3})	T (K)	N	P	E_k/N (K) $r^2n(r)$	Springs
34.61	35.1	256	4	62.10	60.23
		256	8	61.20	61.13
		256	16	60.97	61.71
44.87	9.4	32	4	53.52	31.42
		32	8	46.32	37.97
		32	16	43.88	41.19
		32	32	43.79	42.15
		108	32	42.64	42.02
		32	64	42.12	43.53

of $n(\mathbf{p})$, must be wider, and this is also reflected in the figure.

In Table III, we compare two alternative ways of calculating the kinetic energy within the open polymer algorithm. In the first method, which may be regarded as the equivalent of the experimental procedure (except that there one works with the momentum distribution), we fitted a Gaussian to the single-particle density matrix and derived the kinetic energy from the width of the distribution, i.e., the fit parameter E_k in Eq. (18). The second, conventional method is the (crude) energy estimator, Eq. (6), utilizing the potential energy stored in the intramolecular springs. Note that, in a simulation involving an open polymer, there are only $N-1$ closed polymers, for which spring energies may be calculated. Also, strictly speaking, Eq. (6) does not apply, because it is derived for a ''neat'' system of closed polymers, but the error incurred by using this equation is probably small (of order $1/N$). The general trend, both in the liquid and in the solid, is that the kinetic energies obtained from the intramolecular springs increase monotonically with P, whereas the kinetic energies derived from the width of $n(\mathbf{r})$ decrease with increasing P, but the respective sequences of numbers appear to tend to a common limit. For the liquid, the consistency between the two methods is already very good for $P=8$; for the solid, the respective limits seem to differ by ~ 1 K, but this apparent discrepancy may well be due to the smaller system size or to the rather large uncertainties of the fits (cf. the difference between the $N=32$ and $N=108$ results).

Concluding this section we can state that for neon around 10 K and above, the single-particle density matrix (and, hence, the momentum distribution) are Gaussian to a very good approximation. Therefore, making this assumption the basis of the analysis of experimental data should not lead to significant systematic errors. In simulations, the single-particle density matrix is best calculated using the open polymer algorithm, since this is the only way to ensure that the long-range behavior of $n(\mathbf{r})$ is predicted correctly.

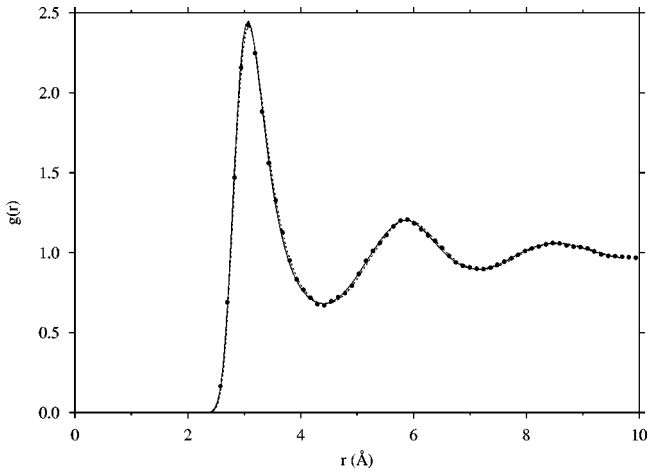

FIG. 7. Pair correlation function $g(r)$ for liquid neon at $\rho = 34.61$ nm^{-3}, $T = 35.1$ K. Circles, experimental result, obtained in Ref. [39] from the neutron scattering data of Ref. [38]; solid line, PIMC simulation using the HFD-C2 potential, $N = 500$ particles, and $P = 32$; dashed line, PIMC simulation using the Lennard-Jones potential.

III. COMPARISON WITH THE NEUTRON SCATTERING EXPERIMENTS

A. The structure factor in the liquid phase

The experimental structure factor of liquid neon was measured long ago by de Graaf and Mozer [38]. The neutron diffraction experiment was quite accurate and the Q range (momentum transfer) covered was such that a reliable radial distribution function could be extracted from the data [39]. A comparison between the experiment and the (quantum corrected) classical simulation can be seen in Ref. [11]. Here, the simulation was carried out using the Wigner-Kirkwood expansion up to the third order (6th power in Λ^*), and a fair quantitative agreement was found between the calculations and the experimental results. However, the agreement was tied to a slight modification of the pair potential parameters. In particular, parameters halfway between the ones derived from gas phase data and those fitted to solid phase properties were found to give the best agreement with the scattering data.

In the present simulation of the liquid, both the LJ and the HFD-C2 potentials were used. For the LJ potential we used the parameters $\varepsilon_{\mathrm{LJ}} = 36.8$ K and $\sigma_{\mathrm{LJ}} = 2.789$ Å [44]. In Fig. 7 we report the $P = 32$ results (cf. Sec. II above) for the radial distribution function and their comparison with the experimental data of de Graaf and Mozer at $T = 35.1$ K, $\rho = 34.61$ nm^{-3}. The agreement between the simulations and the experimental $g(r)$ (using either potential model) is very good over the whole distance range. However, we would expect that a more accurate structure determination should be able to distinguish more clearly between the two potentials [3,4]. A slight discrepancy is observed in the value of the compressibility, which determines the $Q \to 0$ limit of the structure factor. The experimental value for the compressibility yields $S(Q \to 0) = 0.160$. The LJ value is 0.139, while for the HFD-C2 potential it is 0.179 (these numbers were obtained by numerical differentiation of the pressures reported in Table I). The differences between the two simulations, and between the individual simulations and the experiment, are not large but significant, implying that many-body interactions may play a role in liquid neon. Similar features could be noted by comparing the experimental results on the structure factor $S(Q)$ directly with those obtained by Fourier transforming the simulated $g(r)$.

B. The kinetic energy in the liquid phase

The first experimental determination, over a wide range of Q and ω, of the dynamic structure factor $S(Q,\omega)$ of liquid neon at $T = 29.9$ K was published 27 years ago [49]. The high Q values of the scattering function were subsequently analyzed in the framework of NCS theory by Sears [50,51]. However, for this experiment, the highest value for the momentum transfer was $Q = 12.5$ Å^{-1}, which is probably too low for a correct extrapolation of $S(Q,\omega)$ to the impulse approximation regime, $Q \to \infty$.

Some time ago, an experiment at much higher Q values was carried out on liquid neon at $T = 25.8$ and 35.2 K, using the energetic neutrons of a pulsed source [23]. The actual Q range was in the interval 20–28 Å^{-1}, which should justify the use of the impulse approximation theory [52]. The experimental results for the kinetic energy were compared with the available theoretical estimates, which were essentially based on semiclassical expansions of the quantum mechanical operators [23]. More recently, the saturated vapor pressure (SVP) liquid was investigated at $T = 25.8$ K, using the MARI spectrometer at ISIS (U.K.) [40]. Here, the range of the momentum transfer was between 2 and 13 Å^{-1}, but the main goal of the experiment was to gain information on the shape of the momentum distribution.

Our results on the kinetic energy of liquid neon are collected in Table IV, where we have also included previous results obtained within the framework of the Wigner-Kirkwood approximation, to put them in perspective with the present, independent calculations. The formal expansion of the relevant thermodynamic observables of the WK series, up to the second-order term, has been given in Ref. [9]. It is easily seen that the expansion reported by Sears [51] is correct at first order, but he uses an approximate expression for the second-order term that is rigorous only if the spectral density of the velocity autocorrelation function is of Gaussian shape. The column labeled WK1 is the result of a first-order WK calculation that utilizes the experimental $g(r)$ determined in Ref. [38]. The column labeled WK2 is the result of a second-order WK expansion calculation.

First, we note the excellent agreement between the PIMC simulations based on the LJ and the HFD-C2 potential models. The precise form of the interaction potential does not seem to play a substantial role in determining the kinetic energy of liquid neon. This is what we should expect for an observable that is measured by very high energy neutrons probing single-atom properties. Also, the WK calculations are closer to the PIMC values than to the experiment. The same observation applies to the approximate calculation by Sears (WK2 value at $T = 26.9$ K). Moreover, due to the good convergence rate of the WK expansion (cf. footnote b

TABLE IV. Comparison of the various experimental and theoretical determinations of the kinetic energy of liquid neon. For a detailed explanation see Sec. III B.

T	ρ	E_k/N (K)						
(K)	(nm^{-3})	Expt.	Ref.	WK1-LJ	WK2-LJ	PIMC-HFD [d]	PIMC-LJ [e]	Ref.
35.3±0.4	31.70	66.4±3.3	[23]	60 [a]		60.37±0.18	60.25	present work
35.1	32.0				61.7 [b]			[9]
35.1±0.4	34.61	69.0±4.7	[23]	60 [a]		61.44±0.15	61.39	present work
25.8±1.0	36.28	52.8±3.7	[23]	48 [a]		49.71±0.19	49.80	present work
26.9±0.2	36.1	48.2±0.9	[51]		49.7 [c]			[51]

[a]This value was obtained by using the first-order term of the Wigner-Kirkwood expansion and the experimental $g(r)$ from Ref. [38].

[b]Value obtained for the Lennard-Jones model using the Wigner-Kirkwood expansion, up to the second order, according to Ref. [9]. The zeroth-order (classical) term is 52.5 K, the first and second corrections are 8.1 K and 1.1 K, respectively.

[c]Value obtained by Sears [51] using an approximate version of the Wigner-Kirkwood expansion.

[d]Results from the PIMC simulation using the HFD-C2 potential, extrapolated to $P\rightarrow\infty$. The quoted uncertainties are the sum of the difference between the $P=16$ and $P=32$ results and their combined statistical errors, assuming that the former is a measure of the systematic error of the simulations.

[e]Results from the PIMC simulation ($P=32$) using the Lennard-Jones potential.

in Table IV), it appears that a first-order WK calculation should already give reliable results. This is corroborated by the WK1 values that we have calculated using not the simulations but the experimental microscopic structure determined by de Graaf and Mozer [38,39]. Given that the agreement between theory and experiment at the level of the radial distribution function is excellent, this is not surprising.

On the experimental side, the early experimental determination by Sears [51] is found to be in good agreement with the theoretical prediction. However, the more recent experimental data reported in Ref. [23] appear to be systematically higher than all theoretical results. While, at $T=25.8$ K, the experimental value (which has recently been confirmed in Ref. [40]) is still consistent with the simulation result, at the higher temperatures the difference between experiment and simulation exceeds the quoted error margin.

C. The kinetic energy in the solid phase

No experimental data seems to be available on the structure factor of neon in the solid phase. This is to be expected, as a crystal structure develops long-range correlations (Bragg peaks) which render the determination of the diffuse, liquid-like component of the measured $S(Q)$ extremely difficult. However, on the basis of the results obtained for the liquid it is likely that the simulations will also predict the correct structure for the solid phase of neon. Thus, the comparison with experimental neutron scattering data is currently limited to the kinetic energy, values for which have been reported in Refs. [24] and [30]. These experiments were performed at almost constant density and at various temperatures, with the aim of measuring the ground state energy of solid neon. It is worthwhile to note that in Ref. [24] the measured kinetic energies were found to be consistently higher than various theoretical predictions using harmonic models. The authors thus inferred a substantial anharmonicity of neon.

Following the experiment reported in Ref. [24], a paper [41] has appeared that presents the results of a PIMC simulation. This technique is not based on the harmonic hypothesis and therefore one would expect that most of the observed discrepancies should be removed. Instead, a substantial difference was still found between the experimental data and the simulation results. A likely inadequacy of the intermolecular potential (LJ) was then suggested as a possible justification of the discrepancy. The same LJ potential was also used in a subsequent simulation of solid neon [42]. Also, the most recent experiment on solid neon [30] attributed a generally lower value to the atomic kinetic energy and therefore removed most of the previously observed discrepancies. However, the agreement between these experimental data and the simulation results is still not fully satisfactory [30,42]. Therefore, in order to avoid any further source of uncertainty, we decided to perform the present PIMC simulations using the more realistic HFD-C2 potential for neon. These were made at the same temperatures and densities as the experimental determinations [24,30].

In Table V, we report a comparison of various experimental and theoretical results. As far as the consistency of the theoretical calculations is concerned, the present simulations show a substantial agreement for the value of the kinetic energy, using either of two different potentials, namely, HFD-C2 and LJ. This confirms the results already given in Ref. [30], even though the differences are smaller in our case. In general, we find that the present simulation results and those reported in Ref. [30] are in good agreement (~ 1 K) in spite of the different implementation of the PIMC algorithm. The agreement with the results of Refs. [41] and [42] is also good.

By contrast, the experimental results of Ref. [24] appear to be consistently higher than the simulations, with the differences being between two and three times the size of the

TABLE V. Comparison of the various experimental and theoretical determinations of the kinetic energy of solid neon. For a detailed explanation see Sec. III C.

T	ρ			E_k/N (K)		
(K)	(nm^{-3})	Expt.	Ref.	PIMC-HFD	PIMC-LJ	Ref.
4.125	44.97			41.6	42.0	[30]
4.2 ± 0.1	44.97	44.0 ± 1.0	[30]			
4.7 ± 0.1	44.97	49.2 ± 2.8	[24]	41.2 ± 1.1 [a]	40.4 [b]	present work
5.0	44.57				42.81	[41]
9.4 ± 0.1	44.87	49.1 ± 4.0	[24]	41.9 ± 0.3 [a]	42.0 [b]	present work
10.0	44.48				43.21	[41]
10.15	44.85			42.6	43.2	[30]
10.2 ± 0.1	44.68	43.0 ± 1.0	[30]	41.8 ± 0.3 [a]	41.9 [b]	present work
11.4 ± 0.2	44.77	49.0 ± 2.4	[24]	42.5 ± 0.2 [a]	42.7 [b]	present work
15.0	44.11				44.68	[41]
15.2 ± 1.0	44.45	50.0 ± 3.0	[30]			
15.7	44.48			46.5		[30]
17.8 ± 0.2	44.12	51.2 ± 2.8	[24]	45.9 ± 0.1 [a]	46.2 [b]	present work
20.0	43.60				47.68	[41]
20.2 ± 0.1	43.91	48.0 ± 1.0	[30]	47.9 ± 0.2 [a]	48.2 [b]	present work
20.3	43.5			47.8	47.8	[30]
26.4 ± 0.2	43.26	57.9 ± 2.0	[24]	54.1 ± 0.1 [a]	54.5 [b]	present work

[a]Results from PIMC simulations using the HFD-C2 potential, extrapolated to $P\rightarrow\infty$. The quoted uncertainties are the sum of the difference between the $P=32$ and $P=64$ results and their combined statistical errors, assuming that the former is a measure of the systematic error of the simulations.
[b]Results from PIMC simulations ($P=32$) using the LJ potential.

quoted error bars. The more recent results of Ref. [30], however, turn out in a better agreement with the calculations and the differences, when present, never exceed twice the quoted experimental errors. On the average, however, the experiment seems to overestimate the kinetic energy of solid neon (cf., for example, Fig. 3 of Ref. [42]).

Finally, concerning the validity of the WK approximation in the solid phase [53,54], this is questionable and therefore we did not attempt any comparison. In fact, it was already shown (cf. Ref. [9]) that in the solid phase the first correction term in the WK expansion of the kinetic energy was of the same order of magnitude as the classical reference term. In this condition, it is hopeless to expect an asymptotic series to converge.

IV. CONCLUSIONS

The emergence of quantum properties in quasiclassical systems is a process that can be observed gradually in condensed neon. In the liquid state, at relatively high temperatures, quantum effects manifest themselves as a broadening of the single-particle distribution function, $n(\mathbf{r})$. This function degenerates to a δ function in the classical limit but it exhibits a finite width in the quantum mechanical case. The pair distribution function $g(r)$ is only marginally affected by this effect showing just a slight broadening and shift of the first intermolecular peak [11]. Due to the small size of quantum effects in the liquid phase of neon, the results of a previous WK expansion up to the third order in Λ^* were sufficiently accurate to give a fair quantitative agreement with the microscopic structure factor determined from the experiment. However, this involved a slight modification of the pair potential parameters. In the present PIMC calculations, we used two different interatomic potentials, namely, an effective LJ potential and the pure two-body HFD-C2 pair potential, and the simulations give slightly different results for $g(r)$. However, within the present experimental accuracy, it is impossible to discriminate between the two potential models (cf. Fig. 7).

The atomic kinetic energy of neon, on the other hand, has been measured in a much wider density and temperature range. One can use the variation in the kinetic energy to measure the gradual emergence of quantum effects in condensed neon. In fact, the difference between the quantum mechanical kinetic energy and the classical equipartition

theorem increases on decreasing the temperature and becomes very large in the solid phase (cf. Tables IV and V).

The kinetic energy is related to the single-particle distribution function $n(\mathbf{r})$ and its Fourier transform $n(\mathbf{p})$. For a classical particle, $n(\mathbf{p})$ has a Gaussian shape whose width is determined by the thermal kinetic energy $(3/2)k_BT$. As quantum effects become relevant, the value of the kinetic energy deviates from the classical equipartition theorem but the shape of $n(\mathbf{r})$ is usually assumed to remain approximately Gaussian. On the other hand, the Gaussian assumption cannot be retained when quantum statistics starts to play a role, such as in normal helium close to the λ transition or in the superfluid phase [13]. The most recent experiment carried out on liquid neon [40] seems to indicate a marginal deviation of the momentum distribution from a purely Gaussian shape. This suggestion is in contrast with the present simulation results. In fact, we have seen in Figs. 3 and 4, that the Gaussian approximation is very well obeyed by the function $n(\mathbf{r})$, extending for 4–5 orders of magnitude both in the liquid and the solid phase of neon.

As a byproduct of our calculations, we have given a comprehensive comparison between two sets of experimental data and the results of a wide collection of data obtained from quantum simulations of liquid and solid neon. While the structural data show almost perfect agreement between the experiment and the simulation results (liquid phase, cf. Sec. III A), a small systematic difference remains at the level of the kinetic energy, in both the liquid and solid phases.

The theoretical calculations of the ground state kinetic energy of solid neon, which were carried out within the harmonic or the self-consistent harmonic approximation, are in substantial agreement with the simulations (cf. Table II of Ref. [24] and Table V of this paper). The only exception appears to be the variational calculation by Bernardes [55]. However, it should be noted that a subsequent calculation by Nosanow and Shaw [56] (self-consistent solution of Hartree equations) brought that value back to the level of the harmonic models.

Originally, the differences between the experimental data and theory were attributed to a possible high anharmonicity of solid neon. This is not corroborated by the present calculations as all our simulations, i.e., the ones using the LJ potential and those using the HFD-C2 potential, give results in substantial mutual agreement as well as in agreement with the harmonic (or self-consistent harmonic) model.

It was also suggested that three-body irreducible terms in the interaction potential might account, directly or indirectly, for the observed differences in the kinetic energy [24]. We tend to exclude this possibility on the basis of the comparison with the microscopic structure of liquid neon that was shown in Sec. III A. The present results are consistent with the view that three-body irreducible terms in the interaction potentials, when present, show up in the very low Q region of the structure factor $S(Q)$, i.e., at the level of long-range correlations. Alternatively, they may also be observable in certain macroscopic properties such as the equation of state [57]. On the other hand, experiments aiming to measure the kinetic energy of atoms in condensed systems directly involve a very high value of the momentum transfer $\hbar Q$, which is usually chosen in a region where $S(Q)$ is already very close to unity. Therefore, the system is seen by the neutron probe as an ideal gas.

In conclusion, we have presently no explanation for the remaining small difference between the simulated and experimental kinetic energy, both in the liquid and in the solid phase. On the theoretical side, simulations by various groups employing different potential models were found to be in mutual agreement. However, we observe that the uncertainty in the experimental data is still sufficiently large to allow for further improvements, especially at the level of possible systematic errors. In fact, the kinetic energy is measured as the width of the recoil peak in a NCS experiment. This peak, in turn, is convoluted with the instrument resolution function that, at present, is usually large. Therefore, improvements in the instrumental performance could allow better experimental determinations of the kinetic energy. We suggest that the remaining discrepancy found in neon could provide, among other things, a further valid motivation to improve the resolution of the available NCS instruments.

[1] J. P. Hansen and I. R. McDonald, *Theory of Simple Liquids* (Academic Press, New York, 1976).

[2] *Rare Gas Solids*, edited by M. L. Klein and J. A. Venables (Academic Press, London, 1976).

[3] F. Barocchi, P. Chieux, R. Magli, L. Reatto, and M. Tau, Phys. Rev. Lett. **70**, 947 (1993).

[4] M. Zoppi, U. Bafile, E. Guarini, F. Barocchi, R. Magli, and M. Neumann, Phys. Rev. Lett. **75**, 1779 (1995).

[5] R. A. Aziz, in *Inert Gases*, edited by M. L. Klein (Springer-Verlag, Berlin, 1984).

[6] G. Scoles, Annu. Rev. Phys. Chem. **31**, 81 (1980).

[7] J. de Boer, Physica (Utrecht) **14**, 139 (1948).

[8] The definition of the de Boer length parameter is similar to that of the de Broglie wavelength but with the thermal energy k_BT replaced by the potential well depth ε. See, for example, J. de Boer, Rep. Prog. Phys. **12**, 305 (1949).

[9] F. Barocchi, M. Neumann, and M. Zoppi, Phys. Rev. A **36**, 2440 (1987).

[10] J. G. Powles and J. L. F. Abascal, J. Phys. C **16**, L441 (1983).

[11] F. Barocchi, M. Neumann, and M. Zoppi, Phys. Rev. A **31**, 4015 (1985).

[12] E. L. Pollock and D. M. Ceperley, Phys. Rev. B **30**, 2555 (1984).

[13] D. M. Ceperley and E. L. Pollock, Phys. Rev. Lett. **56**, 351 (1986); Can. J. Phys. **65**, 1416 (1987).

[14] D. M. Ceperley, Rev. Mod. Phys. **67**, 279 (1995).

[15] G. Voth, D. Chandler, and V. H. Miller, J. Chem. Phys. **91**, 7749 (1989).

[16] J. Cao and G. Voth, J. Chem. Phys. **99**, 10 070 (1993).

[17] J. Cao and G. Voth, J. Chem. Phys. **100**, 5093 (1994); **100**,

5106 (1994); **101**, 6157 (1994); **101**, 6168 (1994).
[18] G. J. Martyna, J. Chem. Phys. **104**, 2018 (1996).
[19] J. Cao and G. J. Martyna, J. Chem. Phys. **104**, 2028 (1996).
[20] M. Pavese and G. Voth, Chem. Phys. Lett. **249**, 231 (1996); A. Calhoun, M. Pavese, and G. Voth, *ibid.* **262**, 415 (1996).
[21] K. Kinugawa, Chem. Phys. Lett. **292**, 454 (1998).
[22] *Momentum Distributions*, edited by R. N. Silver and P. E. Sokol (Plenum, New York, 1989).
[23] D. A. Peek, M. C. Schmidt, I. Fujita, and R. O. Simmons, Phys. Rev. B **45**, 9671 (1992).
[24] D. A. Peek, I. Fujita, M. C. Schmidt, and R. O. Simmons, Phys. Rev. B **45**, 9680 (1992).
[25] K. W. Herwig, P. E. Sokol, T. R. Sosnick, W. M. Snow, and R. C. Blasdell, Phys. Rev. B **41**, 103 (1990).
[26] T. R. Sosnick, W. M. Snow, and P. E. Sokol, Phys. Rev. B **41**, 11 185 (1990).
[27] C. Andreani, A. Filabozzi, M. Nardone, F. P. Ricci, and J. Mayers, Phys. Rev. B **50**, 12 744 (1994).
[28] J. Bafile, M. Zoppi, F. Barocchi, R. Magli, and J. Mayers, Phys. Rev. Lett. **75**, 1957 (1995).
[29] U. Bafile, M. Zoppi, F. Barocchi, R. Magli, and J. Mayers, Phys. Rev. B **54**, 11 969 (1996).
[30] D. N. Timms, A. C. Evans, M. Boninsegni, D. M. Ceperley, J. Mayers, and R. O. Simmons, J. Phys.: Condens. Matter **8**, 6665 (1996).
[31] V. F. Sears, Can. J. Phys. **63**, 68 (1984).
[32] R. N. Silver, Phys. Rev. B **39**, 4022 (1989).
[33] T. R. Sosnick, W. M. Snow, R. N. Silver, and P. E. Sokol, Phys. Rev. B **43**, 216 (1991).
[34] R. T. Azuah, W. G. Stirling, H. R. Glyde, P. E. Sokol, and S. M. Bennington, Phys. Rev. B **51**, 605 (1995).
[35] R. T. Azuah, W. G. Stirling, H. R. Glyde, M. Boninsegni, P. E. Sokol, and S. M. Bennington, Phys. Rev. B **56**, 14 620 (1997).
[36] K. H. Andersen, W. G. Stirling, and H. R. Glyde, Phys. Rev. B **56**, 8978 (1997).
[37] H. R. Glyde, B. Fåk, and O. Plantevin, J. Low Temp. Phys. **113**, 537 (1998).
[38] L. A. de Graaf and B. Mozer, J. Chem. Phys. **55**, 4967 (1971).
[39] H. J. Raveché and R. D. Mountain, J. Chem. Phys. **57**, 3987 (1972).
[40] R. T. Azuah, W. G. Stirling, H. R. Glyde, and M. Boninsegni, J. Low Temp. Phys. **109**, 287 (1997).
[41] A. Cuccoli, A. Macchi, V. Tognetti, and R. Vaia, Phys. Rev. B **47**, 14 923 (1993).
[42] A. Cuccoli, A. Macchi, G. Pedrolli, V. Tognetti, and R. Vaia, Phys. Rev. B **56**, 51 (1997).
[43] R. A. Aziz, W. J. Meath, and A. R. Allnatt, Chem. Phys. **79**, 295 (1983).
[44] K. Singer and W. Smith, Mol. Phys. **64**, 1215 (1988).
[45] R. P. Feynman, *Statistical Mechanics* (Benjamin, Reading, MA, 1972).
[46] D. Chandler and P. G. Wolynes, J. Chem. Phys. **74**, 4078 (1981).
[47] M. P. Allen and D. J. Tildesley, *Computer Simulation of Liquids* (Clarendon Press, Oxford, 1987).
[48] M. F. Herman, E. J. Bruskin, and B. J. Berne, J. Chem. Phys. **76**, 5150 (1982).
[49] W. J. L. Buyers, V. F. Sears, P. A. Lonngi, and D. A. Lonngi, Phys. Rev. A **11**, 697 (1975).
[50] V. F. Sears, Can. J. Phys. **59**, 555 (1981).
[51] V. F. Sears, Can. J. Phys. **63**, 68 (1985).
[52] V. F. Sears, Phys. Rev. B **30**, 44 (1984).
[53] A. Cuccoli, A. Macchi, M. Neumann, V. Tognetti, and R. Vaia, Phys. Rev. B **45**, 2088 (1992).
[54] M. Asger and Q. N. Usmani, Phys. Rev. B **49**, 12 262 (1994).
[55] N. Bernardes, Phys. Rev. **112**, 1534 (1958).
[56] L. H. Nosanow and G. L. Shaw, Phys. Rev. **128**, 546 (1962).
[57] M. Neumann and M. Zoppi, Phys. Rev. B **62**, 41 (2000).